

1

2     **A 3D simulation of drifting snow in the turbulent boundary layer**

3     **Huang Ning<sup>1,2</sup>, Zhengshi Wang<sup>1,2\*</sup>**

4     <sup>1</sup>Key Laboratory of Mechanics on Disaster and Environment in Western China  
5     (Lanzhou University), The Ministry of Education of China, 730000

6     <sup>2</sup>Department of Mechanics, School of Civil Engineering and Mechanics, Lanzhou  
7     University, Lanzhou, 730000, China

8     \* *Correspondence to:* Zhengshi Wang (Email: wangzhsh2013@lzu.edu.cn)

9 **Abstract.** The drifting snow is one of the most important factors that affect the global  
10 ice mass balance and hydrological balance. Current models of drifting snow are  
11 usually one- or two-dimensional, focusing on the macroscopic quantities of drifting  
12 snow under temporal average flow. In this paper, we take the coupling effects between  
13 wind and snow particles into account and present a 3-D model of drifting snow with  
14 mixed grain size in the turbulent boundary layer. The Large Eddy Simulation (LES)  
15 method is used for simulating the turbulent boundary layer of the wind field and the  
16 3-D trajectory of every motion snow particle is calculated through Lagrangian Particle  
17 Tracking method. Both simulation and experimental results agree well. The results  
18 indicated that the motion trajectories of snow particles, especially the small snow  
19 particles, are obviously affected by the turbulent fluctuation and the particle  
20 movement enhance the turbulent fluctuation in turn. ~~the~~ The visualized observation of  
21 drifting snow in the turbulent boundary layer ~~demonstrates has~~ apparent 3-D structure  
22 and snow streamers, which lead to an intermittent transport of the snow particles and  
23 spatial inhomogeneity. ~~and the motion trajectories of snow particles, especially the~~  
24 ~~small snow particles, are obviously affected by the turbulent fluctuation.~~ The macro  
25 statistics of drifting snow indicates that the variation of spanwise velocity of snow  
26 particles ~~increases with~~ along height depends on the friction velocity and is one order  
27 smaller than that of streamwise velocity. ~~Furthermore, the diameter distribution of~~  
28 ~~snow particles in the air along the height shows a stratification structure.~~

## 29 1 Introduction

30 The phenomenon of the loose snow particles traveling near the land surface under  
31 the action of wind is known as drifting snow. As a typical two-phase flow, drifting  
32 snow is widely distributed in the globe and has significant impacts on the natural  
33 environment and the social economy. On one hand, drifting snow is one of the main  
34 causes of the temporal and spatial variation of snow distribution, contributes greatly  
35 to the mass balance of the ~~Antarctic~~ ice sheets ([Gallée et al., 2013](#)), and further affects  
36 global climate system. The seasonal snow cover also deeply affects the hydrological  
37 balance in cold regions, thus is of glaciological and hydrological importance. On the  
38 other hand, drifting snow causes snow accumulation on the road and reduces visibility,  
39 which may seriously affect the traffic and human activities, and its resultant  
40 non-uniform distribution of snow layer may induce and aggravate various natural  
41 disasters, such as flood, avalanche, mudslides and landslide (Michaux et al.,  
42 [20022001](#)). These disasters may result in not only huge direct and indirect economic  
43 losses, but also human casualties. Thus, in-depth study on the drifting snow is  
44 considered to be essential to comprehensively understanding the ice mass balance and  
45 hydrological balance.

46 The transport processes of snow grains have been extensively investigated  
47 (Pomeroy et al., 1993; [Clifton and Lehning, 2008](#)~~Lehning et al., 2002; Bavay et al.,~~  
48 [2009](#)). Many models were proposed by taking the snow particles as continuous phase  
49 (Uematsu et al., 1993; Mann, 2000; Taylor, 1998; Déry and Yau, 1999; Fukushima et  
50 al., 1999, 2001; Xiao et al., 2000; Bintanja, 2000a, 2000b). ~~Obviously, the above~~  
51 ~~assumption is not in agreement with the real situation. In addition, these models could~~  
52 ~~reveal neither the movement mechanisms of snow particles nor the factors affecting~~  
53 ~~the behaviors of snow particles. These models have a significant role in promoting the~~  
54 ~~drifting snow research although some information can not be acquired from these~~  
55 ~~models, for example, the trajectory of particle and its movement mechanisms.~~  
56 ~~Subsequently~~Recently, Nemoto and Nishimura (2004) studied the snow drifting  
57 process based on particle tracking in a turbulent boundary layer and their 1-D model  
58 included four sub-processes: the aerodynamic entrainment of snow grains, grain-bed  
59 collision, grain trajectories and wind modification. Later, Zhang and Huang (2008)  
60 presented a steady state snow drift model combined with the initial velocity  
61 distribution function and analyzed the structure of drifting snow at steady state.

62 However, neither the details of the spatial variation of snow drifting nor the whole  
63 turbulent structure of wind field can be described due to limitation of their models.  
64 [3-D simulation of drifting snow gradually carried out in recent years. Gauer \(2001\)](#)  
65 [first simulated the blowing and drifting snow in Alpine terrain with Reynolds](#)  
66 [Averaged Navier-Stokes \(RANS\) approaches. Also, Schneiderbauer and Prokop \(2011\)](#)  
67 [developed the SnowDrift3D model based on RANS. Vionnet et al. \(2014\) went on a](#)  
68 [study of large-scale erosion and deposition using a fully coupled](#)  
69 [snowpack/atmosphere model. Groot et al. \(2014\) simulated the small-scale drifting](#)  
70 [snow with a Lagrangian stochastic model based on LES and the intermittency of](#)  
71 [drifting snow was mainly analyzed. Furthermore](#) And, snow particles were uniform  
72 size in most previous models, which is different from the natural situation. To date, a  
73 comprehensive study on drifting snow in the turbulent field is indispensable for a  
74 thorough understanding of the complex drifting snow.

75 In this paper, [based on the model of Dupont et al. \(2013\) that developed for](#)  
76 [blown sand movement, the Advanced Regional Prediction System \(ARPS, version](#)  
77 [5.3.3\), which is a middle-scale meteorological model, is applied in a small-scale for](#)  
78 [drifting snow and a series of adaptations are made for drifting snow simulation. we](#)  
79 ~~We performed a numerical study of present a physical 3-D numerical model for~~  
80 drifting snow in the turbulent boundary layer ~~based on the LES of Advanced Regional~~  
81 ~~Prediction System (ARPS, version 5.3.3)~~ by taking the 3-D motion trajectory of snow  
82 particles with mixed grain size, the grain-bed interaction, and the coupling effect  
83 between snow particles and wind field into consideration and used it to directly  
84 calculate the velocity and position of every single snow particle in turbulent  
85 atmosphere boundary layer, the transport rate and velocity distribution characteristics  
86 of drifting snow, and the mean particles size at different heights. The paper is  
87 structured as follows: Section 2 briefly introduces the model and methods; [Section 3](#)  
88 [illuminates the model validations;](#) Section ~~3-4~~ presents the simulation results and  
89 discussions, and Section ~~4-5~~ is the conclusion.

## 90 **2 Model and Methods**

### 91 **2.1 Turbulent boundary layer**

92 The ARPS developed by University of Oklahoma is a three-dimensional,  
93 non-hydrostatic, compressible LES model and has been used for simulating wind soil  
94 erosion (Vinkovic et al., 2006; Dupont et al., 2013). In this paper, it is used for

95 modeling the drifting snow.

96 Snow saltation movement in the air is a typical two-phase movement, in which  
 97 the coupling of particles and the wind field is a key issue. [Vinkovic et al. \(2006\)](#)  
 98 [introduced the volume force caused by the particles into Navier-Stokes equation of](#)  
 99 [ARPS and](#) The conservation equations of momentum and subgrid scale (SGS)  
 100 turbulent kinetic energy (TKE) after filtering ~~with considering the impact of the~~  
 101 ~~presence of particles on the flow field~~ can be expressed as (Vinkovic et al., 2006;  
 102 Dupont et al., 2013):

$$103 \quad \frac{\partial \tilde{u}_i}{\partial t} + \tilde{u}_j \frac{\partial u_i}{\partial x_j} = -\frac{1}{\bar{\rho}} \frac{\partial}{\partial x_i} (\tilde{p}'' - \alpha_{div} \frac{\partial \bar{\rho} \tilde{u}_j}{\partial x_i}) - g \left( \frac{\tilde{\theta}''}{\theta} - \frac{c_p}{c_v} \frac{\tilde{p}''}{\bar{p}} \right) \delta_{i3} - \frac{\partial \tau_{ij}}{\partial x_j} - f_i \quad (1)$$

$$104 \quad \frac{\partial e}{\partial t} + \tilde{u}_j \frac{\partial e}{\partial x_j} = -\tau_{ij} \frac{\partial \tilde{u}_i}{\partial x_j} + \frac{\partial}{\partial x_j} \left( 2 \left( (1 - \delta_{j3}) v_{th} + \delta_{j3} v_{tv} \right) \frac{\partial e}{\partial x_j} \right) \\ - \frac{g}{\theta} \tau_{3\theta} - \varepsilon - \frac{1}{V_{grid}} \sum_{s=1}^{N_p} \frac{m_p}{\bar{\rho}} \frac{2e}{T_p + T_L} f(Re_p)$$

105 where the tilde symbol indicates the filtered variables and the line symbol represents  
 106 grid volume-averaged variables.  $x_i$  ( $i=1,2,3$ ) stand for the streamwise, lateral, and  
 107 vertical directions, respectively,  $u_i$  refers to the instantaneous velocity component of  
 108 three directions,  $\delta_{ij}$  is the Kronecker symbol,  $\alpha_{div}$  means the damping coefficient,  
 109  $p$  and  $\rho$  are the pressure and density of air, respectively;  $g$  is the gravity  
 110 acceleration,  $\theta$  indicates the potential temperature,  $c_p$  and  $c_v$  are the specific heat  
 111 of air at constant pressure and volume, respectively;  $t$  is time,  $\tau_{ij}$  denotes the  
 112 subgrid stress tensor, and  $f_i$  is the drag force caused by the particles and can be  
 113 written as (Yamamoto et al., 2001):

$$114 \quad f_i = \frac{1}{\rho V_{grid}} \sum_{s=1}^{N_p} m_p \frac{u_i(x_p(t), t) - u_{pi}(t)}{T_p} f(Re_p) \quad (3)$$

115 where  $V_{grid}$  is the grid cell volume,  $N_p$  stands for the number of particles per grid,  
 116  $m_p$  means the mass of particles,  $u_{pi}(t)$  and  $u_i(x_p(t), t)$  represent the velocity of  
 117 particles and the wind velocity at grain location at time  $t$ , respectively, and  $f(Re_p)$   
 118 is an empirical relation of the particle Reynolds number  $Re_p$  (Clift et al., 1978):

$$\begin{aligned}
 f(Re_p) &= 1 & (Re_p < 1) \\
 f(Re_p) &= 1 + 0.15Re_p^{0.687} & (Re_p \geq 1)
 \end{aligned} \tag{4}$$

In the equation (2),  $e$  is the SGS TKE,  $\nu_{ih}$  and  $\nu_{iv}$  stand for the horizontal and vertical eddy viscosities, respectively,  $\tau_{3\theta}$  is the subgrid heat flux, and  $\varepsilon$  indicates the dissipation rate of SGS TKE.  $T_p$  and  $T_L$  represent the particle response time and the Lagrangian correlation timescale, respectively, and can be expressed as

$$T_p = \frac{\rho_p d_p^2}{18\rho\nu} \quad \text{and} \quad T_L = \frac{4e}{3C_0\varepsilon} \tag{5}$$

where  $C_0$  is the Lagrangian constant and  $\nu$  denotes the molecular kinematic viscosity.

## 2.2 Governing equation of particle motion

Because snow particles have much higher density  $\rho_p$  than air ( $\rho_p/\rho \approx 10^3$ ) and much smaller diameter  $d_p$  than Kolmogorov scale, in ~~this~~ simulation, they are approximately regarded as a sphere and only possess gravity and drag force. Thus, their motion governing equation can be expressed as (Vinkovic et al., 2006)

$$\frac{d\bar{x}_p(t)}{dt} = \bar{v}_p(t) \tag{6}$$

$$\frac{d\bar{v}_p(t)}{dt} = \frac{\bar{v}(\bar{x}_p(t), t) - \bar{v}_p(t)}{T_p} f(Re_p) + \bar{g} \tag{7}$$

where  $\bar{v}_p(t)$  and  $\bar{v}(\bar{x}_p(t), t)$  are the velocity of the particle and the fluid velocity of particle position at time  $t$ , respectively.

It is worth noting that the inertia effect of snow particles is considered by evaluating the maximum particle response time, so the particle motion is the dynamical calculation of time step, which is guaranteed to be less than the maximum particle response time.

## 2.3 Grain-bed interactions ~~Rebound and splash~~

### 2.3.1 Aerodynamic Entrainment

Snow particles will be entrained into the air if the shear force produced by air flow is large enough. The number of entrainment  $N$  (per unit area per unit time) can be express as (Anderson and Haff, 1991):

$$N = \eta(\tau - \tau_t) \tag{8}$$

带格式的：正文，定义网格后自动调整右缩进，行距：单倍行距，到齐到网格

带格式的：字体：Times New Roman，小四，降低量 3 磅

带格式的：降低量 6 磅

带格式的：字体：Times New Roman，小四

带格式的：正文，右，定义网格后自动调整右缩进，行距：单倍行距，允许文字在单词中间换行，到齐到网格

146 where  $\tau$  is the local surface shear stress and  $\tau_t$  is the threshold shear stress.

147 Obviously, if  $\tau$  of every position in the computation domain is always smaller than  
148  $\tau_t$ , no particle can start-up and the drifting snow will not happened. The threshold  
149 shear stress can be described as

$$\tau_t = A^2 g d (\rho_p - \rho) \quad (9)$$

151 in which  $A = 0.2$  is more suited to snow as reported by Clifton et al. (2006).

152 The coefficient takes the form of  $\eta = C / (8\pi d_p^2)$  (Doorschot and Lehning, 2002)

153 and  $C = 1.5$ .

154 The initial velocity of entrained particles follows a lognormal distribution with  
155 mean value  $3.3u_*$  ( $u_*$  is the friction velocity), which is consistent with the  
156 measurements of saltating snow in wind tunnel (Nishimura and Hunt, 2000) and has  
157 been adopted by drifting snow studies (Clifton and Lehning, 2008; Groot et al., 2014).  
158 And the initial take-off angle can be described by a lognormal distribution with a  
159 mean value of  $(75 - 55(1 - \exp(-\langle d_p \rangle / 1.75 \times 10^{-4})))$  (Clifton and Lehning, 2008).

160 The collision of saltating particles with the bed surface is a key physical process in  
161 saltation, as it will rebound with a certain probability and may splash new saltating  
162 particles into the air (Shao and Lu, 2000). Kok and Renno (2009) have proposed a  
163 physical splashing function based on the conservation of energy and momentum. Thus,  
164 the saltation process under various physical environments can be accurately simulated  
165 and applied to the mixed soils and drifting snow.

### 2.3.1.2 Rebounding

167 The grain bed interaction is a stochastic process, in which the impact When a  
168 moving particles impact on the bed, it may rebound into air again may rebound with a  
169 certain probability. If a particle rebounds into the air, it can be described using three  
170 variables: the velocity  $v_{reb}$ , the angle toward the surface  $\alpha_{reb}$  and the angle toward a  
171 vertical plane in the streamwise direction  $\beta_{reb}$ .

172 The rebound probability can be expressed as (Anderson and Haff, 1991):

$$P_{reb} = B[1 - \exp(-\gamma v_{imp})] \quad (10)$$

带格式的: 字体: Times New Roman, 小四

带格式的: 字体: Times New Roman, 小四, 降低量 3 磅

带格式的: 字体: Times New Roman, 小四, 降低量 6 磅

带格式的: 正文, 定义网格后自动调整右缩进, 行距: 单倍行距, 到齐到网格

带格式的: 正文, 右, 定义网格后自动调整右缩进, 行距: 单倍行距, 到齐到网格

带格式的: 字体: Times New Roman, 降低量 7 磅

带格式的: 字体: Times New Roman, 小四

带格式的: 正文, 右侧: 0.85 厘米, 定义网格后自动调整右缩进, 行距: 单倍行距, 到齐到网格

带格式的: 字体: Times New Roman, 小四, 非加粗

174 where  $v_{imp}$  is the impact velocity of particle,  $B$  and  $\gamma$  are the experienced  
175 parameters. Here,  $\gamma = 2s / m$  and  $B = 0.90$  are employed as Groot et al.(2014)  
176 indicate that these value are more accurate for drifting snow.

177 ~~where  $v_{imp}$  is the impact velocity of particle,  $B$  and  $\gamma$  are the experienced~~  
178 ~~parameters. Here,  $B = 0.95$  and  $\gamma = 2s / m$  are employed.~~

179 Recent experiment shows that the fraction of kinetic energy retained by the  
180 rebounding particle approximately follows normal distribution (Wang et al., 2008):

$$181 \text{prob}(v_{reb}^2) = \frac{1}{\sqrt{2\pi}\sigma_{reb}} \exp\left(-\frac{(v_{reb}^2 - \langle v_{reb}^2 \rangle)^2}{2\sigma_{reb}^2}\right) \quad (11)$$

182 where  $\langle v_{reb}^2 \rangle = 0.45v_{imp}^2$  and  $\sigma_{reb} = 0.22v_{imp}^2$  (Kok and Renno, 2009).

183 The angle  $\alpha_{reb}$  approximately follows an exponential distribution. Although Kok  
184 and Renno (2009) suggest the mean value of  $\alpha_{reb}$  is  $45^\circ$  and it was used by Groot  
185 et al. (2014) for drifting snow, we choose a mean value depending on the mean  
186 particle size because many researches indicate that  $\alpha_{reb}$  relay on particle size (Rice  
187 et al., 1995; Zhou et al., 2006):

188 ~~For the velocity after rebound  $v_{reb}$ , Kok and Renno (2009) indicate that the~~  
189 ~~fraction of kinetic energy retained by the rebounding particle approximately follows~~  
190 ~~normal distribution as follow:~~

$$191 v_{reb}^2 = ((45 \pm 22)\%)v_{imp}^2 \quad (11)$$

192 ~~Two angles are introduced in the rebound process to describe the rebound~~  
193 ~~direction as mentioned above. The angle  $\alpha_{reb}$  approximately follows an exponential~~  
194 ~~distribution. Although it is not affected by the impact velocity, it decreases~~  
195 ~~exponentially with the increase of particle diameter (Rice et al., 1995; Zhou et al.,~~  
196 ~~2006). The relationship of average value of rebound angle to particle diameter can be~~  
197 ~~expressed as:~~

$$198 \langle \alpha_{reb} \rangle = 161.46e^{-\frac{d_p}{250 \times 10^{-6}}} + 0.15 \quad (12)$$

199 where  $d_p$  is measured in the unit of micrometer.

200 However, the angle  $\beta_{reb}$  was rarely involved in previous studies and may not

带格式的：缩进：首行缩进： 1.5 字符

201 strongly affect the saltation process ( Dupont et al., 2013). Here we choose  
 202  $\beta_{reb} = 0^\circ \pm 15^\circ$ .

### 203 **2.3.2.3 Splashing**

204 The newly ejected particles and the ‘dead particles’ (not rebounded) will reach  
 205 equilibrium when the saltation process becomes stable.

206 The number of newly ejected particles is usually proportional to the impact  
 207 velocity and can be written as (Kok and Renno, 2009):

$$208 \quad N = \frac{a}{\sqrt{gD}} \frac{m_{imp}}{\langle m_{ej} \rangle} v_{imp} \quad (13)$$

209 where  $a$  is a dimensionless constant in the range of 0.01–0.05. This value affect the  
 210 ‘saturation length’ (total transport rate of drifting snow reached equilibrium) to a great  
 211 extent. We find that  $a = 0.03$  is closer to the observation of drifting snow in the wind  
 212 tunnel (Okaze et al., 2012). While this parameter will not influence the steady state of  
 213 drifting snow because we found the percentage of eject particles is always less than  
 214 3% in the fully developed drifting snow.  $D$  is the typical particle size ( $\langle d_p \rangle$  in this  
 215 paper),  $m_{imp}$  is the mass of impacting particle and  $\langle m_{ej} \rangle$  is the average mass of  
 216 ejection grains. ~~where  $a$  is a dimensionless constant in the range of 0.01–0.05 (here~~  
 217  ~~$a = 0.03$ ),  $D$  is the typical particle size ( $\langle d_p \rangle$  in this paper,  $m_{imp}$  is the mass of~~  
 218 ~~impacting particle and  $\langle m_{ej} \rangle$  is the average mass of ejection grains.~~

219 Once a new particle is splashed into the air, it can also be characterized by its  
 220 velocity  $v_{ej}$ , its angle toward the surface  $\alpha_{ej}$  and its angle toward a vertical plane in  
 221 the streamwise direction  $\beta_{ej}$ .

222 The speed of the ejected particles is exponentially distributed. Kok and Renno  
 223 (2009) developed a physical expression of the average dimensionless speed of the  
 224 ejected particle as follow:

$$225 \quad \frac{\langle v_{ej} \rangle}{\sqrt{gD}} = \frac{\langle \lambda_{ej} \rangle}{a} \left[ 1 - \exp\left(-\frac{v_{imp}}{40\sqrt{gD}}\right) \right] \quad (14)$$

226 where  $\langle \lambda_{ej} \rangle$  is the average fraction of impacting momentum applied on the ejecting  
 227 surface grains. We choose  $\langle \lambda_{ej} \rangle = 0.15$  in this paper, which corresponds to the

228 [experimental observation of sand by Rice et al. \(1995\).](#)

229 ~~where  $\langle \lambda_{ej} \rangle$  is the average fraction of impacting momentum applied on the ejecting~~  
230 ~~surface grains. We choose  $\langle \lambda_{ej} \rangle = 0.15$  in this paper.~~

231 Kok and Renno (2009) indicated that the angle  $\alpha_{ej}$  approximately follows an  
232 exponential distribution and its mean value is  $50^\circ$ , ~~which was also adopted by Groot~~  
233 ~~et al. (2014).~~ In addition, the angle  $\beta_{ej} = 0^\circ \pm 15^\circ$ , ~~similar to Dupont et al. (2013).~~

234 ~~$$\beta_{ej} = 0^\circ \pm 15^\circ$$~~

## 235 **2.4 Simulation Details**

236 ~~In this paper we have performed some wind tunnel experiments to obtain the~~  
237 ~~initialization data for the simulation as well as to compare the simulated results with~~  
238 ~~experiment results. The The blowing snow process in the turbulent boundary layer is~~  
239 ~~simulated and the simulation results are compared with the existent experiment results.~~  
240 ~~Computational computational~~ region is set as  $16m \times 1.0m \times 1.5m$  and divided into  
241 two sections, as show in Figure 1. The first zone ~~extending from  $x = 0m$  to  $x = 5m$~~  is  
242 ~~used for the development of the fully developed turbulent wind field region with a~~  
243 ~~steady turbulent boundary layer and provides a steady turbulent boundary~~  
244 ~~layer extending from  $x = 0m$  to  $x = 5m$  and a flow field cycle at  $x = 1m$ . In this~~  
245 ~~simulation, the turbulent characteristics separating from our wind tunnel results are~~  
246 ~~added on the initial logarithmic velocity profile at beginning and the inlet velocity of~~  
247 ~~fluid will be equal to the wind velocity at the location of  $x = 5m$  after 5 seconds~~  
248 ~~which realizes a long distance development of the turbulent boundary layer. The~~  
249 second zone is the ~~blowing snow blowing~~ region from  $x = 6m$  to  $x = 16m$ , where a  
250 ~~sufficient~~ loose snow layer is set on the ground.

251 In this model, the grid has a uniform size of  $\Delta x = \Delta y = 0.05m$  in the horizontal  
252 direction, and the average mesh size of  $\Delta z = 0.03m$  in the vertical direction. The grid  
253 is stretched by cubic function to acquire ~~more~~ detailed information of the surface  
254 layer and the smallest grid is  $\Delta z_{min} = 0.002m$ .

255 ~~A turbulent boundary layer over a snow bed is generated using~~ ~~The actual~~  
256 ~~computation time is 30 seconds, in which the first 10s and the second 10s are~~  
257 ~~respectively used for the development of turbulent boundary layer and the drifting~~  
258 ~~snow, and the last 10s for data statistics. The dynamic Smagorinsky-Germano~~

带格式的：缩进：首行缩进： 0 字符，定义网格后自动调整右缩进，行距：单倍行距，到齐到网格

带格式的：字体：Calibri，五号

带格式的：字体：Times New Roman，小四，非倾斜

带格式的：缩进：首行缩进： 0 字符

259 | subgrid-scale (SGS) model ~~is used in the simulation. by setting the soil type,~~  
260 | ~~reasonable roughness and an initial field with turbulent fluctuations.~~ For the flow field,  
261 | we applied the rigid ground boundary condition at the bottom, the open radiation  
262 | boundary in the top, the periodic boundary condition in the spanwise direction, the  
263 | open radiation boundary condition at the end of the domain along the streamwise  
264 | direction. ~~The forced boundary is applied in the inflow as mentioned above. –and the~~  
265 | ~~periodic boundary condition in the inflow with the cycle location at  $x=5.0m$ . The~~  
266 | ~~initial wind database is obtained from the experimental results of wind tunnel.~~  
267 | Additionally, The the snow particles have circulatory motion in the lateral boundary  
268 | and they will disappear when moving out of the outlet in the end of the domain.

269 | The size distribution of snow particles in this paper is fitted to the experiment  
270 | results obtained from field observations of SPC (Schmidt, 1984), that is

$$271 | f(d_p) = \frac{d_p^{(\alpha-1)}}{\beta^\alpha \Gamma(\alpha)} \exp(-d_p / \beta) \quad (15)$$

272 | where  $\alpha$  and  $\beta$  are the shape and scale parameters of gamma-function distribution  
273 | and we choose a value of 4.65 and 75.27, respectively. Every new ejection or  
274 | entrainment particle will be given a random size from above distribution and will be  
275 | tracked separately. The sizes of snow particles in the air are stochastically collected  
276 | and the size distribution is presented in figure 2. The mean diameter is about  
277 |  $\langle d_p \rangle = 350 \mu m$ . The results are in consistence with those observational results of the  
278 | natural snow (Omiya et al., 2011).~~where  $\alpha$  and  $\beta$  are the shape and scale~~  
279 | ~~parameters of gamma function distribution, respectively. Here, the diameters of 2617~~  
280 | ~~snow particles are counted and their distribution is presented in Figure 2. The mean~~  
281 | ~~diameter is  $\langle d_p \rangle = 350 \mu m$ . The results are in consistence with those observational~~  
282 | ~~results of the natural snow (Omiya et al., 2011).~~

283 | The density of snow particles and air are  $912 kg / m^3$  and  $1.225 kg / m^3$ ,  
284 | respectively. And the surface roughness and the molecular kinematic viscosity of  
285 | snow particles are  $z_0 = \langle d_p \rangle / 30$  and  $\nu = 1.5 \times 10^{-5}$ , respectively. ~~Several particles~~  
286 | ~~will be forced to take off from bed surface with random velocities ( $u_{pi} = (0-1)m/s$ )~~  
287 | ~~at random positions in the domain at the initial moment of drifting snow.~~

288 | The processes of snow blowing with the friction wind velocity of

带格式的：首行缩进： 0 字符

289  $u_* = 0.179 \sim 0.428 \text{ m/s}$  are performed with the environmental temperature of  
290  $-10^\circ\text{C}$  and initial relative humidity of 90%. And we found the lower bound of friction  
291 velocity for a drifting snow is approximately  $0.18 \text{ m/s}$  for this situation.The  
292 ~~processes of snow blowing with the wind velocity of  $u_* = 0.179 \sim 0.428 \text{ m/s}$  are~~  
293 ~~performed at environmental temperature of  $-10^\circ\text{C}$  and initial relative humidity of~~  
294 ~~90%.~~

### 295 **3 Model validations**

296 The wind profile is firstly obtained by the time averaging and spatial averaging  
297 of a time-series of wind velocities ( $t = 5 \sim 10 \text{ s}$  and the time interval is  $0.01 \text{ s}$ ). As  
298 shown in figure 3, the method leads to similar wind profiles to that of wind tunnel  
299 experiment at different wind speeds.

300 Snow transport rate (STR) is one of the most important indicators of the strength  
301 of the drifting snow. Figure 4(a) shows the evolution of STR per width along  
302 streamwise in different friction wind velocity. It can be seen that the STR per width  
303 increases along with the streamwise and gradually reaches a steady state, which is  
304 basically consistent with the observation in the wind tunnel by Okaze et al. (2012).  
305 And it appears that the distance needed to reach the state is increase with the  
306 increasing of friction wind speed. The STR per width (averaging from  $x = 14 \text{ m}$   
307 to  $x = 15 \text{ m}$ ) versus friction velocity is presented in figure 4(b). It can be observed  
308 that the STR per width increases with friction wind velocity increasing. The  
309 relationship of STR per width  $Q$  and friction velocity  $u_*$  can be expressed as

$$310 \quad \underline{Q = 1.94u_*^{4.51}}$$

311 which is consistent with the experiment results of Sugiura et al. (1998) and the  
312 simulation results of Nemoto and Nishimura (2004).

313 Then, figure 5 shows the relationship of STR per unit area to the saltation height.  
314 As shown in figure 5, the variations in the STR per unit area with height at different  
315 friction wind speeds are equivalent, that is, the STR per unit area decreases with  
316 height increasing. The comparison of the simulation and experiment results of Sugiura  
317 et al. (1998) is also displayed in the inset map of figure 5 and they are in a good  
318 agreement.

319 Subsequently, the velocity distribution of snow particles in the air is shown in

带格式的: 缩进: 首行缩进: 0 字符

320 figure 6, in which (a) is the average velocity of snow particles along the streamwise  
321 direction as a function of height and (b) displays the corresponding velocity  
322 probability distribution of snow particles. It can be observed from figure 6(a) that the  
323 average velocity of snow particles along the streamwise direction increases with the  
324 height increasing, in which the experiment data has been calibrated by wind speed.  
325 Good accordance with the experimental results until below 0.02m mainly because  
326 mid-air collision near bed surface is high frequency and loses energy.

327 It can be seen from figure 6(b) that the probability distribution of snow particles'  
328 velocity along the streamwise direction obeys the unimodal distribution. In other  
329 words, it distributes mainly at 0 ~ 4 m / s and the amount of snow particles moving in  
330 the opposite direction is basically less than 3% of the total snow particles. Meanwhile,  
331 the probability distribution basically does not change with the friction wind speed, in  
332 agreement with our experiment. It should be noted that the high-speed particles in this  
333 simulation are significantly more than those captured in the experiments (figure 6(b)).  
334 This is mainly because the mean velocity of snow particles increases with height  
335 increasing, our measurement is mainly set at lower positions due to the limitation of  
336 instrument and thus part of high-speed particles are not being captured.

337 A more detailed statistics of the percentages of particles that moving at different  
338 velocities are showed in figure 6(c). The field observation of Greeley et al. (1996)  
339 showing that the proportions of saltating sand particles with velocity smaller than  
340 1.5m / s and greater than 4 m / s are greater than 59% and smaller than 3%,  
341 respectively. However, the proportion of snow particles with the velocity smaller than  
342 1.5m / s is in general smaller than 48% and the percentage of particles with velocity  
343 greater than 4 m / s increase with the increasing friction velocity. It can be found  
344 that the drifting snow has more high-speed particles than saltating sand, which is  
345 mainly because the density of snow particles are significant smaller than sand and  
346 they are more easily suspended and followed.

347 Finally, figure 7 shows the mean size of snow particles along height in the air at  
348 different friction velocities and compared with the experimental result of Gromke et al.  
349 (2014). All the data have been normalized to the average diameter of overall snow  
350 particles. It is clearly that the mean diameter of snow particles in the saltation layer  
351 slightly decreases with the height increasing, which is also consistent with the  
352 observation of previous works (Nishimura and Nemoto, 2005). However, it appears

353 that the mean diameter increase with increasing height above the saltation layer. The  
354 main reason may be that the small particle trends to carry smaller inject velocity,  
355 while the larger particle is just the opposite due to the stronger inertia. The rebound  
356 velocity is proportional to the incident velocity and thus larger snow particle will  
357 rebound with a bigger initial velocity.

### 358 **3.4 Results and discussions**

#### 359 **3.4.1 Analysis of the flow field** The interaction between turbulent and particle 360 motion

361 Almost all the flows at atmospheric boundary layer are turbulent. ~~Therefore, the~~  
362 ~~simulation of turbulent boundary layer is the key and basis for accurately simulating~~  
363 ~~the drifting snow. Enough time is supplied for forming a stable turbulent boundary~~  
364 ~~layer before particles taking off. The computational region is relative small and the~~  
365 ~~inflow contains the real turbulent fluctuation.~~ The turbulent fluctuations will affect the  
366 movement of snow particles and the particle motion will influence the development of  
367 turbulent.

368 Figure 3-8 shows the cloud map of velocity along the streamwise direction  
369 ( $u_x = 0.428 m/s$ ) (a) before the snow particles take off ( $t=5s$ 10s) and (b) when the  
370 drifting snow has been sufficiently developed ( $t=20s$ 25s). The slice ~~elicited by arrows~~  
371 displays the velocity cloud map of ~~U-U~~-direction at height  $H = 0.001 m$ . Figures  
372 38(a-1) and 38(a-2) show the contour surface map ( $\pm 0.5 m/s$ ) of wind velocity along  
373 spanwise direction and vertical direction, respectively, at time  $t = 10s$ , and ~~Figures~~  
374 ~~figures~~ 38(b-1) and 38(b-2) show the corresponding results at time  $t = 25s$ . At the  
375 same time, the typical trajectories of snow particles are represented in figure 9, in  
376 which the diameter of (a) and (b) are  $100 \mu m$  and  $300 \mu m$ , respectively. The blue  
377 dotted line denotes the motion trajectory that is not affected by the turbulence and it is  
378 calculated by another drifting snow model (Zhang and Huang, 2008) with the same  
379 take-off velocity and wind profile.

380 It can be seen from figure 9 that turbulence can significantly affect the  
381 trajectories of snow particles with diameter smaller than  $100 \mu m$ , and may drive these  
382 snow particles moving up to 5~6 m during one saltation process. By contrast, the  
383 trajectories of larger snow particles are less affected by the turbulent fluctuation,  
384 showing only slight influence on the saltation height, saltation distance and landing  
385 position of snow particles. This is consistent with the sand saltation in the turbulent

带格式的: 缩进: 首行缩进: 0 字符

boundary layer performed by Dupont et al. (2013). On the other hand, we can see from figure 10 that the wind velocity is significantly decreased in the drifting snow region due to the reaction force of the snow particles, while the TKEs are obviously enhanced during snow drifting. This result is attributed to the fact that velocity gradient is obviously changed when the drifting snow formed (Okaze et al., 2012).

~~It can be observed from Figure 3 that homogeneous turbulent fluctuations are distributed in the fully developed boundary layer. When the stable drifting snow is formed, the wind velocity will significantly decrease in the drifting snow region due to the reaction force of the snow particle and the turbulent fluctuations gradually become non-uniform in the drifting snow region. This is mainly due to the presence of the snow streamers resulted great difference in the number concentration of snow particles at different positions (details are shown in Section 3.2).~~

~~In addition to the turbulent fluctuation, the wind profile can also be obtained by the time averaging and spatial averaging of a time series of wind velocities ( $t = 3 - 5 s$  and the time interval is  $0.01 s$ ). As shown in Figure 4, the method leads to similar wind profiles to that of wind tunnel experiment at different wind speeds.~~

~~When the turbulent boundary layer is fully developed, the snow particles will be released and the motion feature of snow particles could be further obtained.~~

### **3.2.1 The formation of Snow snow streamers**

The saltation process, either in the field or in the wind tunnel, exhibits a temporospatial discontinuity. This discontinuity is affected by many factors such as turbulent fluctuation, topography, surface moisture, roughness elements, etc (Stout and Zobeck, 1997; Durán et al., 2011). ~~Different from Most previous models which are unable to clearly describe the drifting snow structure, our 3-D model could be used to directly calculate the The 3-D motion trajectory of every snow particle is calculated and further intuitively demonstrate the overall structure of snow saltation layers could be intuitively demonstrated~~ because it describes the macroscopic performance of a large amount of drifting snows saltating particles.

Figure 5(a) and 5(b) show the typical trajectories of snow particles with diameter of  $100 \mu m$  and  $300 \mu m$ , respectively, in which the blue dotted line denotes the motion trajectory that is not affected by the turbulence. It can be seen that turbulence can significantly affect the trajectories of snow particles with diameter smaller than  $100 \mu m$ , and may drive snow particles with diameter of  $100 \mu m$  moving  $5 - 6 m$  during one

419 saltation process. By contrast, the trajectories of larger snow particles are less affected  
420 by the turbulent fluctuation, showing only slight influence on the saltation height,  
421 saltation distance and landing position of snow particles.

422 A large amount of snow particles move complexly in the turbulent boundary layer,  
423 constituting the overall structure of the drifting snow. Figure 6 shows the top view of  
424 the snow driving particles concentration and the horizontal cloud map of streamwise  
425 wind velocity at corresponding moment, in which, (a) and (b) represent the moment  
426 of  $t=8\text{ s}$  and  $t=12\text{ s}$ , respectively.

427 It can be observed from Figure 6-11 that snow streamers with high saltating  
428 particle concentration obviously swing forward along the downwind direction,  
429 merging or bifurcating during the movement. It can also be found that the snow  
430 streamers with elongated shape differ greatly in length, but only 0.1~0.2 m in width.  
431 From the corresponding slices of wind velocity cloud map, it can be seen that many  
432 low-speed streaks exist in the near-wall region of the turbulent boundary layer. By  
433 comparing the concentration and corresponding velocity cloud map, it is hard to  
434 decide the relationship between particle concentration and local wind velocity, which  
435 is just like the sand streamers reported by Dupont et al. (2013). This may be due to the  
436 complex motion of the snow particles and hysteretic change of local wind. However,  
437 the shapes of snow streamers are quite different from that of sand streamers. For  
438 example, the snow streamers trend to be longer and thinner in the turbulent boundary  
439 layer. it can be found that the particle concentration shows a direct proportional  
440 relationship with the local wind velocity, that is, only few snow particles present in  
441 the low speed streaks.

442 The in-homogeneous take off and splash of the snow particles in the turbulent  
443 wind field are the main reasons for the formation of snow streamers. The shape and  
444 size of streamers largely depend on the flow structure of the turbulent boundary layer.  
445 In addition, during the full development of drifting snow, the saltating particles and  
446 wind field are in the state of dynamic balance due to the feedback effect of each other.  
447 When the number concentration of snow particles at a certain position is high enough,  
448 the local wind velocity will be significantly reduced, resulting in a lower splash level.  
449 Thus the streamer will gradually weaken or even disappear. In contrast, the local wind  
450 speed in the low concentration region will increase, which enhances the splash  
451 process, so the snow particles will grow rapidly and form a streamer. Furthermore, the

452 fluctuating velocity may also change the movement direction of snow particles. All  
453 the above reasons together cause the serpentine forward of the snow streamers.

### 454 **3.3 Snow transport rate**

455 ~~Snow transport rate (STR) is one of the most important indicators of the strength of~~  
456 ~~the drifting snow. In this simulation, the snow particles will be collected if they pass~~  
457 ~~through the section located at  $x=3\text{ m}$  during the time of  $t=10\text{--}20\text{ s}$ . Figure 7(a)~~  
458 ~~shows the time evolution of STR per width in different friction wind velocity. It can~~  
459 ~~be seen that the STR per width increases rapidly and reaches a dynamic equilibrium~~  
460 ~~state in a short time. With the friction wind speed increasing, the time needed to reach~~  
461 ~~the equilibrium state also increases. During the transport process, STR per width also~~  
462 ~~slightly fluctuates and its fluctuation amplitude is proportional to the friction wind~~  
463 ~~velocity, mainly owing to the intermittent behavior of drifting snow. At the same time,~~  
464 ~~it can be observed from Figure 7(b) that the STR per width increases with friction~~  
465 ~~wind velocity increasing, in consistence with the existing experiment results.~~

466 ~~The average particle concentrations under different friction wind velocities as a~~  
467 ~~function of height are shown in Figure 8(a). It is clear from the figure that the average~~  
468 ~~particle concentrations at different friction wind velocity similarly fluctuate with~~  
469 ~~height, that is, they decrease with height increasing. And the greater the friction wind~~  
470 ~~velocity, the greater the maximum height the snow particles can achieve. Further~~  
471 ~~analysis shows that the difference of average particle concentrations under different~~  
472 ~~friction wind speed is proportional to height. For example, at the height of 0.001 m,~~  
473 ~~the average particle concentration at friction wind velocity of  $u_* = 0.361\text{ m/s}$  is 2.86~~  
474 ~~times greater than that at friction wind velocity of  $u_* = 0.215\text{ m/s}$ ; while at the~~  
475 ~~height of 0.2 m, the former is 176.32 times greater than the latter. Therefore, it is~~  
476 ~~concluded that the significant increase of snow particles at the higher position is the~~  
477 ~~major contributor to the increase of STR at higher wind speed mainly because the~~  
478 ~~snow particles in the higher-speed flow field can acquire more energy from the air and~~  
479 ~~will rebound with a higher velocity.~~

480 ~~Figure 8(b) shows the relationship of STR per unit area to the saltation height. As~~  
481 ~~shown in Figure 8(b), the variations in the STR per unit area with height at different~~  
482 ~~friction wind speeds are equivalent, that is, the STR per unit area decreases with~~  
483 ~~height increasing. However, the STRs per unit area differ greatly at the same height at~~  
484 ~~different friction wind speeds. In the same condition, the STRs per unit area at height~~

485  ~~$h=0.01$  m under friction wind velocity of  $u_* = 0.215$  m/s,  $u_* = 0.252$  m/s ;~~  
486  ~~$u_* = 0.288$  m/s and  $u_* = 0.361$  m/s are  $0.028$  kg/m<sup>2</sup>/s,  $0.057$  kg/m<sup>2</sup>/s ;~~  
487  ~~$0.102$  kg/m<sup>2</sup>/s and  $0.378$  kg/m<sup>2</sup>/s, respectively.~~

### 488 **3.44.3 Velocity of snow particles**

489 As one of the most important aspects to evaluate the accuracy of a drifting snow  
490 model, the velocity information (especially in the spanwise direction) of snow  
491 particles in the air is worthy of attention although it is seldom given in previous  
492 models. ~~The location and velocity of every snow particle can be obtained, and the~~  
493 ~~most important of all, the spanwise velocity of snow particles can be directly obtained~~  
494 ~~in our simulation. The velocity distribution of snow particles in the air and the initial~~  
495 ~~take-off velocity of the ejected particles are given in Section 3.4.1 and Section 3.4.2,~~  
496 ~~respectively.~~

#### 497 **3.4.1 Velocity of snow particles in the air**

498 ~~The velocity distribution of snow particles in the air is shown in Figure 9, in~~  
499 ~~which (a) is the average velocity of snow particles along the streamwise direction as a~~  
500 ~~function of height and (b) displays the corresponding velocity probability distribution~~  
501 ~~of snow particles. It can be observed from Figure 9(a) that the average velocity of~~  
502 ~~snow particles along the streamwise direction increases with the height increasing and~~  
503 ~~with the friction wind velocity at the same height increasing. It can be seen from~~  
504 ~~Figure 9(b) that the probability distribution of snow particles' velocity along the~~  
505 ~~streamwise direction obeys the unimodal distribution. In other words, it distributes~~  
506 ~~mainly at  $0-3$  m/s and the amount of snow particles moving in the opposite~~  
507 ~~direction is less than 3% of the total snow particles. Meanwhile, the probability~~  
508 ~~distribution does not change with the friction wind speed, in agreement with our~~  
509 ~~experiment. In this work, at friction wind velocity of  $u_* = 0.288$  m/s, the proportions~~  
510 ~~of snow particles with the velocity smaller than  $1.5$  m/s and greater than  $4$  m/s are~~  
511 ~~65.07% and 1.76%, respectively, consistent with a field observation of Greeley et al.~~  
512 ~~(1996) showing that the proportions of saltating particles with velocity smaller than~~  
513  ~~$1.5$  m/s and greater than  $4$  m/s are greater than 59% and smaller than 3%,~~  
514 ~~respectively.~~

515 It should be noted that the high speed particles in our simulation are significantly  
516 more than those captured in the experiments (Figure 9(b)). This is mainly because the

517 ~~concentration of snow particles decreases with height increasing, making it~~  
518 ~~increasingly difficult to be captured the high-speed snow particles.~~

519 Firstly, the spanwise velocity of snow particles in the air is analyzed. As shown  
520 in Figure-figure 10-11 shows the spanwise velocity of snow particles in the air, where  
521 (a) is the distribution of the absolute value of spanwise velocity along the elevation  
522 and (b) is the corresponding probability distribution of snow particles' velocity. It is  
523 observed from figure 12(a) that the mean velocity along spanwise basically increases  
524 with the increasing wind speed. This can also be certified from figure 12(b) that the  
525 proportion of snow particles in the air with higher spanwise velocity increases with  
526 friction velocity increasing. Furthermore, it can be seen that when the friction velocity  
527 is small, the absolute value of spanwise velocity increases-decreases with increasing  
528 height; while the law is just the opposite for large friction velocity. And the  
529 spanwise velocity of snow particles is in-an order of magnitude less than that of the  
530 streamwise in general-velocity. The variation in the spanwise velocity with height at  
531 different friction wind velocity is not obvious. The main reason for this is that  
532 turbulent fluctuations are fairly minimal when the wind speed is small, and they exert  
533 an increasingly stronger with the growing wind speed.

534 ~~From the above analysis it is quite evident that the velocity distribution of snow~~  
535 ~~particles in the air is not sensitive to the wind velocity. The main reason for that is the~~  
536 ~~wind velocity in the full development drifting snow slightly varies due to the reaction~~  
537 ~~force of snow particles in the air.~~

#### 538 **3.4.2 Take-off velocity of snow particles**

539 Then, the The initial take-off velocities-speed distributions of snow particles in  
540 three directions are acquired due to they are (including rebound particles) widely used  
541 in the numerical model. The probability distributions of lift-off velocity in a fully  
542 developed drifting snow field are presented in Figure 11-13, in which the (a), (b), (c)  
543 and (d) show the distributions of streamwise, spanwise, vertical and resultant  
544 velocities, respectively. It is clear that all the velocity components obey the unimodal  
545 distribution. The vertical lift-off velocity -and-are is basically not affected by the  
546 friction wind velocity while the initial take-off speed along streamwise and spanwise  
547 trend to increase with the increasing wind speed. This provides a reference for use the  
548 probability distributions of initial take-off speed.

549 ~~Although there is no obvious difference in take-off velocity at different wind~~  
550 ~~velocity, we can see that a large amount of particles may saltate at higher saltation~~

带格式的: 首行缩进: 0 字符

551 ~~height and greater friction wind speed. It may be inferred that turbulent fluctuation~~  
552 ~~plays an important role in the lifting of snow particles.~~

### 553 **3.5 Diameter distribution of snow particles in the air**

554 ~~The snow particles with mixed size close to natural situation are applied in our~~  
555 ~~simulation. In this section, the size distribution of snow particles in the air is analyzed.~~

556 ~~Figure 12 shows the size distributions of snow particles in the air at different~~  
557 ~~friction velocities, and their comparison with the experimental results. All the data~~  
558 ~~have been normalized to the average of overall snow particles due to different~~  
559 ~~characteristics of snow particles in different experiments. To avoid the random error,~~  
560 ~~those data with snow particle influx less than  $10^4$  ( $\text{m}^{-2}\text{s}^{-1}$ ) have been eliminated. It is~~  
561 ~~clearly that the mean diameter of snow particles near ground (with height below 0.05~~  
562 ~~m) is unchanged with the height increasing, which is consistent with the conclusion~~  
563 ~~obtained by Gromke et al. (2014). However, the mean diameter of snow particles with~~  
564 ~~height above 0.05 m exhibits a growing trend with height increasing, similar to the~~  
565 ~~results observed by Sedmit (1984). This is mainly because larger particles withstand~~  
566 ~~greater drag force in the air during the movement process and have higher impact~~  
567 ~~velocity. Therefore, they will rebound with higher initial velocity because the rebound~~  
568 ~~velocity is proportional to the incident velocity.~~

## 569 **4.5 Conclusions**

570 ~~In this study, the we establish a 3-D drifting snow model process with mixed~~  
571 ~~particle size in the turbulent boundary layer is performed, simulate the development~~  
572 ~~process of drifting snow with mixed particle size and draws the following main~~  
573 ~~conclusions:~~

574 (1) Turbulent fluctuation may significantly affect the trajectory of small snow  
575 particles with equivalent diameter  $d_p \leq 100 \mu\text{m}$ , while has little influence on that of  
576 particles with larger size. And the saltating particles can strengthen the turbulent  
577 fluctuation.

578 (2) ~~The drifting snow in a turbulent boundary layer is very intermittent.~~ Fully  
579 developed drifting snow swings forward toward the downwind in the form of snow  
580 streamers and the wind velocity is proportional to the concentration of snow particles  
581 at different locations of the turbulent boundary layer.

582 (3) The change of spanwise velocities of snow particles along streamwise and  
583 spanwise directions increase with the height rely on the friction velocity, and the

584 ~~latter spanwise velocity~~ is one order of magnitude less than the ~~former streamwise~~  
585 ~~direction~~ in general. ~~In addition, the velocity distribution is not sensitive to the wind~~  
586 ~~speed.~~

587 ~~(4) The mean diameter of snow particles in the air is obviously distributed in~~  
588 ~~layers. It is constant for snow particles with height less than 0.05 m, but shows a~~  
589 ~~gradual increase trend for snow particles with height above 0.05 m.~~

590

591 *Acknowledgements.* This work is supported by the State Key Program of National  
592 Natural Science Foundation of China (91325203), the National Natural Science  
593 Foundation of China (11172118, 41371034), and the Innovative Research Groups of  
594 the National Natural Science Foundation of China (11121202), National Key  
595 Technologies R & D Program of China (2013BAC07B01).

596

## 597 **References**

598 [Anderson, R. S., and Haff, P. K.: Wind modification and bed response during saltation](#)  
599 [of sand in air, \*Acta Mech.\*, 1, 21–51, 1991.](#)

600 Bavay, M., Lehning, M., Jonas, T., and Lowe, H.: Simulations of future snow cover  
601 and discharge in Alpine head water catchments, *Hydrological Processes*, 23(1),  
602 95-108, 2009.

603 Bintanja, R.: Snowdrift suspension and atmospheric turbulence. Part I: Theoretical  
604 background and model description, *Boundary-Layer Meteorology*, 95(3),  
605 343-368, 2000a.

606 Bintanja, R.: Snowdrift suspension and atmospheric turbulence. Part II: Results of  
607 Model Simulations, *Boundary-Layer Meteorology*, 95(3), 369-395, 2000b.

608 Clift, R., Grace, J. R., and Weber, M. E.: *Bubbles, Drops and Particles*, Academic,  
609 New York, 1978.

610 [Clifton, A, Rüedi, J-D., and Lehning, M.: Snow saltation threshold measurements in a](#)  
611 [drifting snow wind tunnel, \*J. Glaciol.\*, 39, 585–596, 2006.](#)

612 [Clifton, A., and Lehning, M.: Simulations of wind tunnel snow drift using a](#)  
613 [semi-stochastic model, \*Earth. Surf. Process. Landforms\*, 33\(14\), 2156-2173,](#)  
614 [doi:10.1002/esp.1673, 2008.](#)

615 Déry, S., and Yau, M. K.: A Bulk Blowing Snow Model *Boundary-Layer,*  
616 *Meteorology*, 93(2), 237-251, 1999.

617 Dupont, S., Bergametti, G., Marticorena, B., and Simoëns, S.: Modeling saltation

带格式的: (中文) 中文(中国)

618 intermittency, *J. Geophys. Res.*, 118(13), 7109-7128, 2013.

619 Durán, O., Claudin, P., and Andreotti, B.: On aeolian transport: Grain-scale  
620 interactions, dynamical mechanisms and scaling laws *Aeolian Research*, 3(3),  
621 243-270, 2011.

622 Fukushima, Y., Etoh, T., Ishiguro, S., Kosugi, K., and Sato, T.: Fluid dynamic analysis  
623 of snow drift using a non-Boussinesq  $k-\varepsilon$  turbulence model (in Japanese with  
624 English abstract), *Seppyo*, 63, 373-383, 2001.

625 Fukushima, Y., Fujita, K., Suzuki, T., Kosugi, K., and Sato, T.: Flow analysis of  
626 developing snowdrifts using a  $k-\varepsilon$  turbulence model (in Japanese with English  
627 abstract), *Seppyo*, 61, 285-296, 1999.

628 [Gallée, H., Trouvilliez, A., Agosta, C., Genthon, C., Favier, V., and Naaim-Bouvet, F.:  
629 Transport of Snow by the Wind: A Comparison Between Observations in Adélie  
630 Land, Antarctica, and Simulations Made with the Regional Climate Model MAR,  
631 \*Boundary-Layer Meteorol.\*, 146,133-147, DOI 10.1007/s10546-012-9764-z,  
632 2013.](#)

633 [Gauer, P.: Numerical modeling of blowing and drifting snow in Alpine terrain, \*J.\*  
634 \*Glaciol.\*, 47\(156\), 97–110, doi: 10.3189/172756501781832476, 2001.](#)

635 Greeley, R., Blumberg, D. G., and Williams, S. H.: Field measurements of the flux and  
636 speed of wind-blown sand, *Sedimentology*, 43(1), 41-52, 1996.

637 Gromke, C., Horender, S., Walter, B., and Lehning, M.: Snow particle characteristics  
638 in the saltation layer, *Journal of Glaciology*, 60, 431-439, 2014.

639 [Groot Zwaaftink, C. D., Diebold, M., Horender, S., Overney, J., Lieberherr, G.,  
640 Parlange M., and Lehning, M.: Modelling small-scale drifting snow with a  
641 Lagrangian stochastic model based on large-eddy simulations, \*Bound. Layer\*  
642 \*Meteorol.\*, 153, 117-139, DOI:10.1007/s10546-014-9934-2, 2014.](#)

643 Kok, J. F., and Renno, N. O.: A comprehensive numerical model of steady state  
644 saltation (COMSALT), *J. Geophys.Res.*, 114(D17), D17204, 2009.

645 ~~[Lehning, M., Bartelt, P., Brown, B., and Fierz, C.: A physical SNOWPACK  
646 model for the Swiss avalanche warning Part III: meteorological forcing,  
647 thin layer formation and evaluation, \*Cold Regions Science and\*  
648 \*Technology\*, 35, 169-184, 2002.](#)~~

649 Mann, G. W., Anderson, P. S., and Mobbs, S. D.: Profile measurements of  
650 blowing snow at Halley, Antarctica, *J. Geophys. Res.*, 105, 24491-24508,

651 2000.

652 [Michaux, J. L., Naaim-Bouvet, F., and Naaim, M.: Drifting-snow studies over an](#)  
653 [instrumented mountainous site: II. Measurements and numerical model at small](#)  
654 [scale, \*Annals of Glaciology\*, 32\(1\), 175-181, 2001.](#)

655 ~~[Michaux, J. L., Naaim-Bouvet, F., Kosugi, K., Sato, A. and Sato, T.: Study in a](#)  
656 [climatic wind tunnel \(Cryospheric Environment Simulator\) of the influence of](#)  
657 [the type of grain of snow and of the flow on the formation of a snow drift, \*La\*](#)  
658 [Houille Blanche Revue Internationale De l'Eau, \(6-7\), 79-83, 2002.](#)~~

659 Nemoto, M., and Nishimura, K.: Numerical simulation of snow saltation and  
660 suspension in a turbulent boundary layer, *J. Geophys. Res.*, 109, D18206, 2004.

661 [Nemoto, M., and Nishimura, K.: Numerical simulation of snow saltation and](#)  
662 [suspension in a turbulent boundary layer, \*J. Geophys. Res.\*, 109, D18206, 2004.](#)

663 [Nishimura, K., Hunt, J. C. R.: Saltation and incipient suspension above a flat particle](#)  
664 [bed below a turbulent boundary layer, \*J. Fluid Mech.\*, 417, 77-102, 2000.](#)

665 [Nishimura, K., and Nemoto, M.: Blowing snow at Mizuho station, Antarctica, \*Phil.\*](#)  
666 [Trans. R. Soc. A, 2005, 363, doi: 10.1098/rsta.2005.1599, 2005.](#)

667 [Sugiura, K., Nishimura, K., Maeno, N., and Kimura, T.: Measurements of snow mass](#)  
668 [flux and transport rate at different particle diameters in drifting snow, \*Cold\*](#)  
669 [Regions Science and Technology, 27\(2\), 83-89,](#)  
670 [doi.org/10.1016/S0165-232X\(98\)00002-0, 1998.](#)

671 Omiya, S., Sato, A., Kosugi, K., and Mochizuki, S.: Estimation of the electrostatic  
672 charge of individual blowing-snow particles by wind tunnel experiment, *Annals*  
673 *of Glaciology*, 52(58), 148-152, 2011.

674 [Okaze, T., Mochida, A., Tominaga, Y., Nemoto, M., Sato, T., Sasaki, Y., and Ichinohe,](#)  
675 [K.: Wind tunnel investigation of drifting snow development in a boundary layer,](#)  
676 [\*J. Wind Eng. Ind. Aerodyn.\*, 104\(106\), 532-539, 2012.](#)

677 Pomeroy, J. W., Gray, D. M., and Landine, P. G.: The Prairie Blowing Snow Model:  
678 characteristics, validation, operation, *Journal of Hydrology*, 144(1-4), 165-192,  
679 1993.

680 Rice, M. A., Willetts, B. B., and McEwan, I. K.: An experimental study of multiple  
681 grain-size ejection produced by collisions of saltating grains with a flat bed,  
682 *Sedimentology*, 42(4), 695-706, 1995.

683 Schmidt, R. A.: Measuring particle size and snowfall intensity in drifting snow, *Cold*

684 Regions Science and Technology, 9(2), 121-129, 1984.

685 [Schneiderbauer, S., Prokop, A.: The atmospheric snow-transport model: SnowDrift3D,](#)  
686 [Journal of Glaciology, 52\(203\), 526-542, 2011.](#)

687 [Shao, Y., and Lu, H.: A simple expression for wind erosion threshold friction velocity,](#)  
688 [J. Geophys. Res., 105\(D17\), 22437-22443, 2000.](#)

689 Stout, J. E., and Zobeck, T. M.: Intermittent saltation, *Sedimentology*, 44(5), 959-970,  
690 1997.

691 [Sugiura, K., Nishimura, K., Maeno, N., Kimura, T., Measurements of snow mass flux](#)  
692 [and transport rate at different particle diameters in drifting snow, Cold Regions](#)  
693 [Science and Technology, 27\(2\), 83-89, 1998.](#)

694 Taylor, P.: The Thermodynamic Effects of Sublimating, Blowing Snow in the  
695 Atmospheric Boundary Layer, *Boundary-Layer Meteorology*, 89(2), 251-283,  
696 1998.

697 [Tominaga, Y., Okaze, T., Mochida, A., Sasaki, Y., Nemoto, M., and Sato, T.: PIV](#)  
698 [measurements of saltating snow particle velocity in a boundary layer developed](#)  
699 [in a wind tunnel, Journal of Visualization, 16\(2\), 95-98, 2013.](#)

700 Uematsu, T., Nakata, T., Takeuchi, K., Arisawa, Y., and Kaneda, Y.:  
701 Three-dimensional numerical simulation of snowdrift, *Cold Regions Science and*  
702 *Technology*, 20(1), 65-73, 1991.

703 Vinkovic, I., Aguirre, C., Ayrault, M. and Simoëns, S.: Large-eddy Simulation of the  
704 Dispersion of Solid Particles in a Turbulent Boundary Layer, *Boundary-Layer*  
705 *Meteorology*, 121(2), 283-311, 2006.

706 [Vionnet, V., Martin, E., Masson, V., Guyomarc'h, G., Naaim-Bouvet, F., Prokop, A.,](#)  
707 [Durand, Y., and Lac, C.: Simulation of wind-induced snow transport and](#)  
708 [sublimation in alpine terrain using a fully coupled snowpack/atmosphere model,](#)  
709 [The Cryosphere, 8, 395-415, doi:10.5194/tc-8-395-2014, 2014.](#)

710 [Wang, D., Wang, Y., Yang, B., and Zhang, W.: Statistical analysis of sand grain/bed](#)  
711 [collision process recorded by high-speed digital camera, Sedimentology, 55\(2\),](#)  
712 [461-470, doi:10.1111/j.1365-3091.2007.00909.x., 2008.](#)

713 Xiao, J., Bintanja, R., Déry, S., Mann, G, and Taylor, P.: An intercomparison among  
714 four models of blowing snow *Boundary-Layer Meteorology*, 97(1), 109-135,  
715 2000.

716 Yamamoto, Y., Potthoff, M., Tanaka, T., Kajishima, T., and Tsuji, Y.: Large-eddy  
717 simulation of turbulent gas-particle flow in a vertical channel: effect of

带格式的：分散对齐

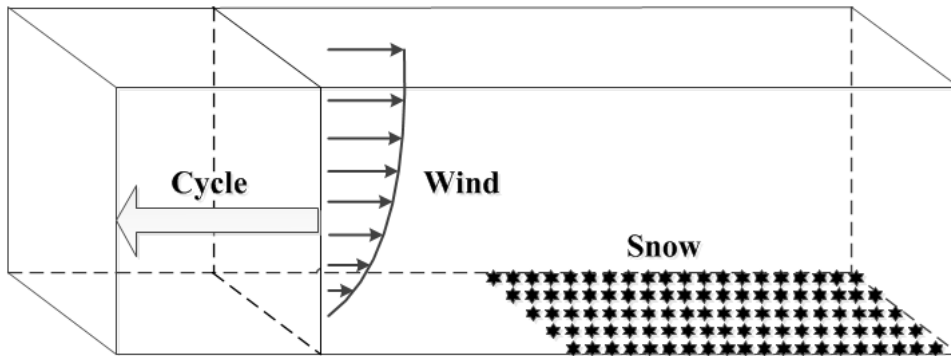
带格式的：缩进：左 2 字符，首  
行缩进： 0 字符

718            considering inter-particle collisions, *Journal of Fluid Mechanics*, 442, 303-334,  
719            2001.

720    Zhang, J., and Huang, N.: Simulation of Snow Drift and the Effects of Snow Particles  
721            on Wind, *Modeling and Simulation in Engineering*, 408075-408076, 2008.

722    Zhou, Y. H., Li, W. Q., and Zheng, X. J.: Particle dynamics method simulations of  
723            stochastic collisions of sandy grain bed with mixed size in aeolian sand saltation,  
724    J. Geophys. Res., 111(D15), D15108, 2006.

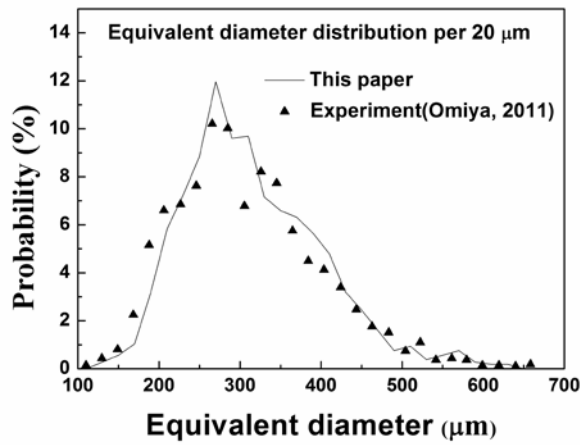
725 **Figures:**



726

727

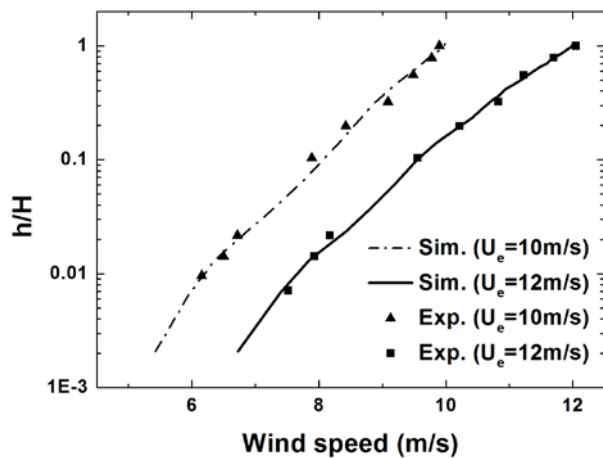
**Figure 1.** Diagram of computational region.



728

729

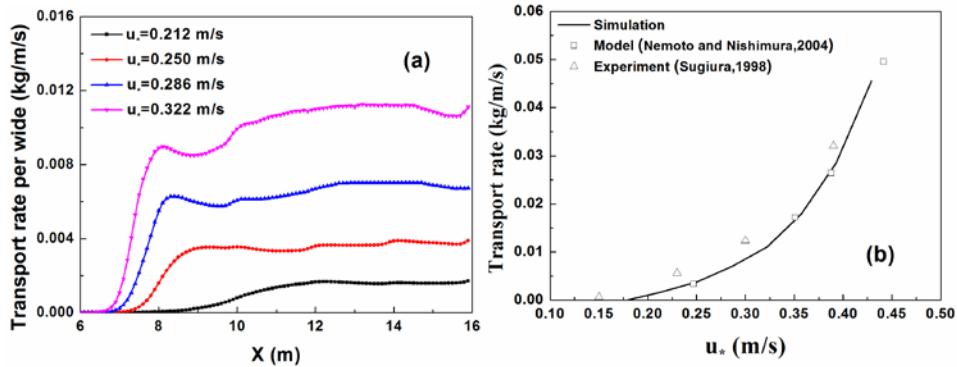
**Figure 2.** Equivalent diameter probability distribution of snow particles.



730

731

**Figure 3.** The wind profile at (a)  $U_e=10\text{m/s}$  and (b)  $U_e=12\text{m/s}$ .

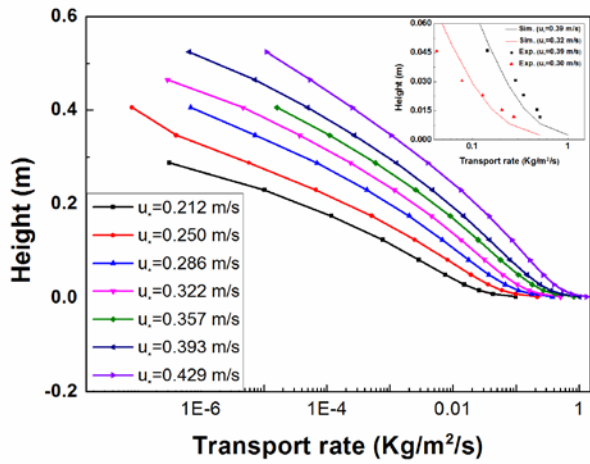


732

733

**Figure 4.** Variation of the snow transport rate (STR) per width with (a) development distance and (b) friction wind velocity.

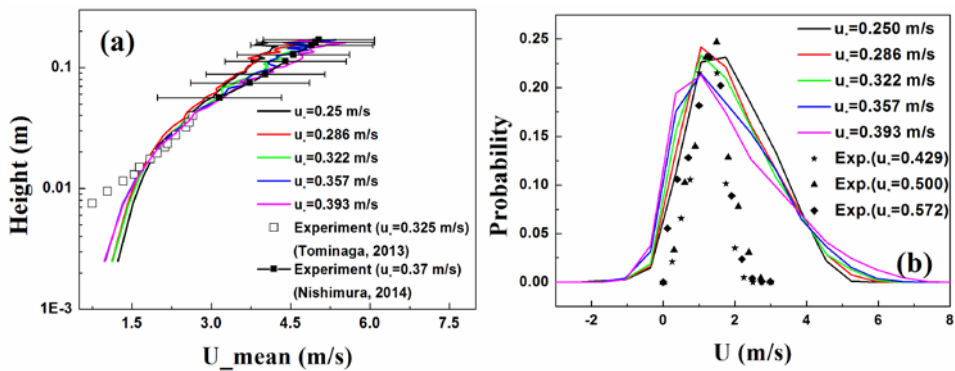
734



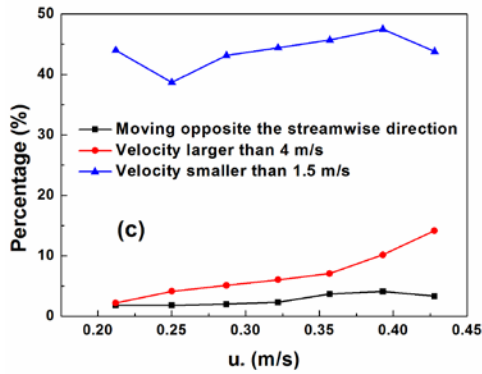
735

736

**Figure 5.** The STR per unit area versus height at different friction wind velocities.



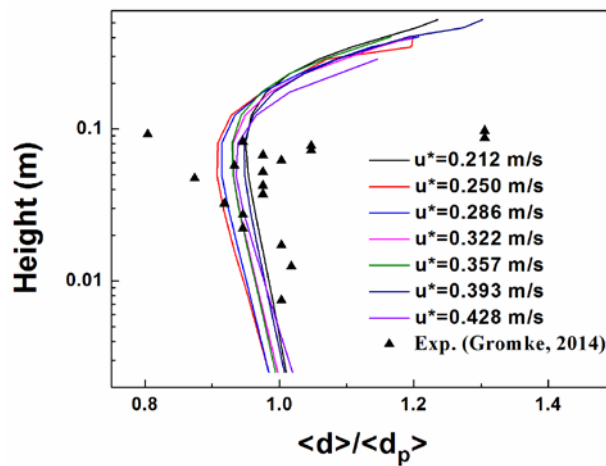
737



带格式的: 左

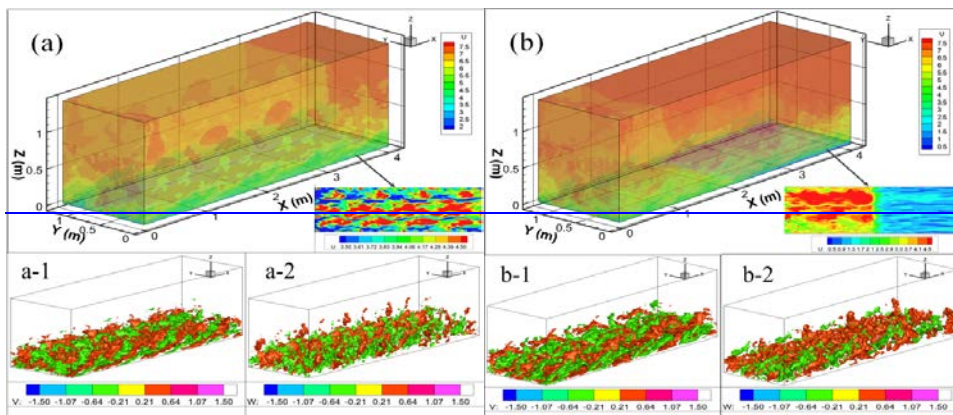
738

739 Figure 6. (a) Variation of the average velocity of snow particles along streamwise  
 740 direction as a function of height, (b) the velocity probability distribution of snow  
 741 particles and (c) the percentage of particles in different velocity vs friction wind  
 742 velocities.

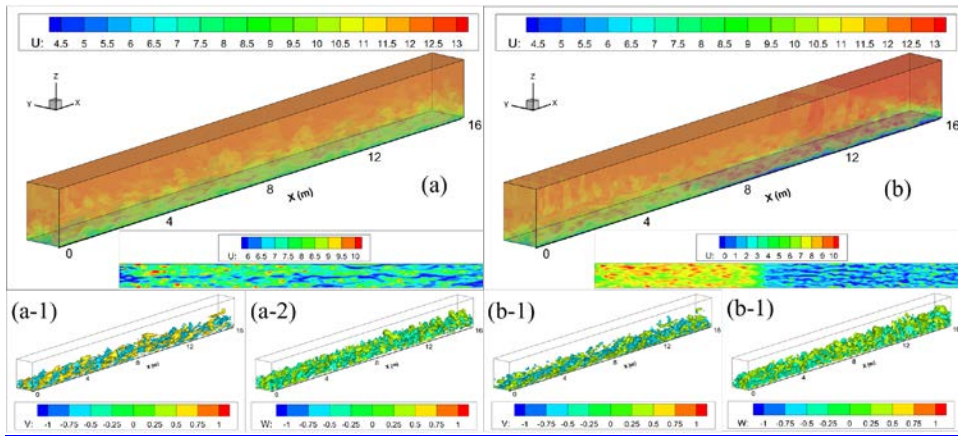


743

744 Figure 7. The mean equivalent diameter distribution of snow particles in the air vs  
 745 height.

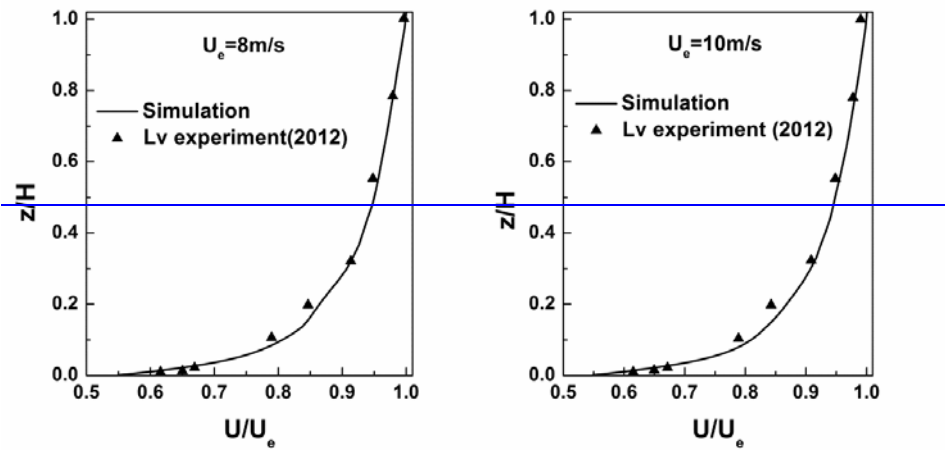


746



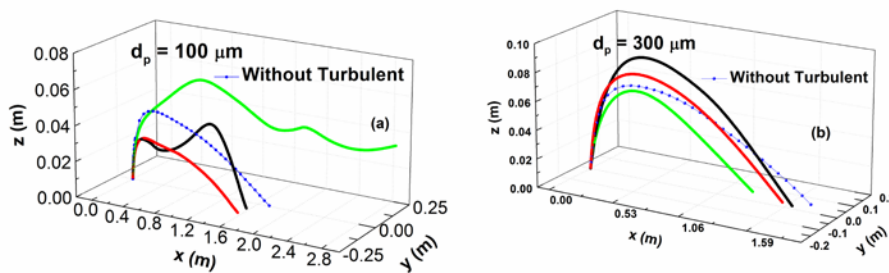
747  
748

Figure 38. The cloud map of flow field at (a)  $t=5s-10s$  and (b)  $t=20s-25s$ .



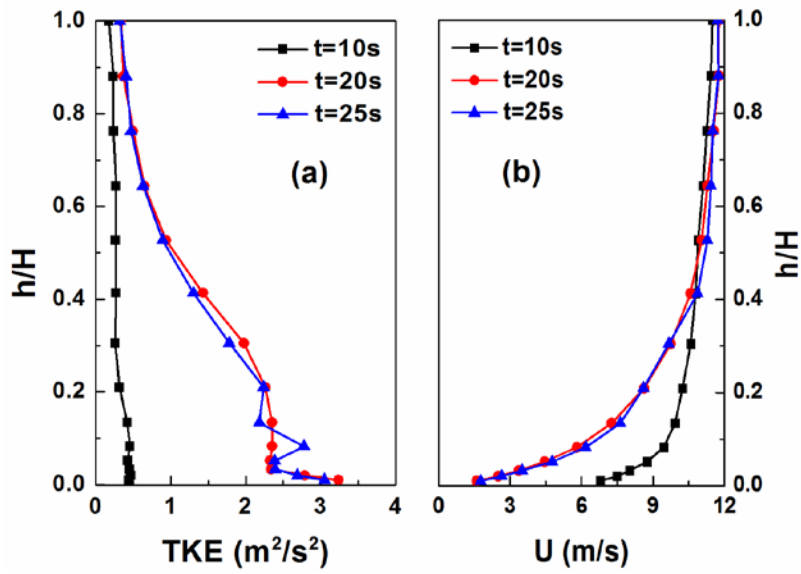
749  
750

Figure 4. The wind profile at (a)  $U_e=8m/s$  and (b)  $U_e=10m/s$ .



751  
752  
753  
754

Figure 59. The 3-D trajectories [schematic diagram](#) of snow particles with different diameters ( $u_* = 0.35 m/s$ ).



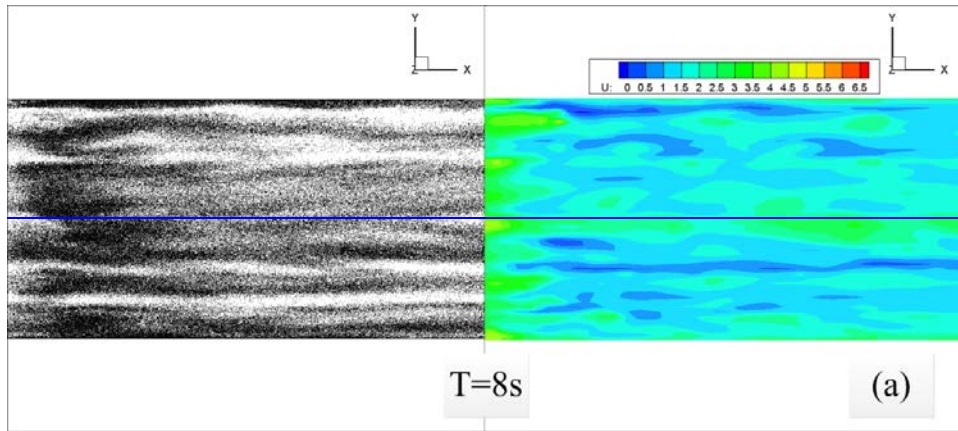
755

756

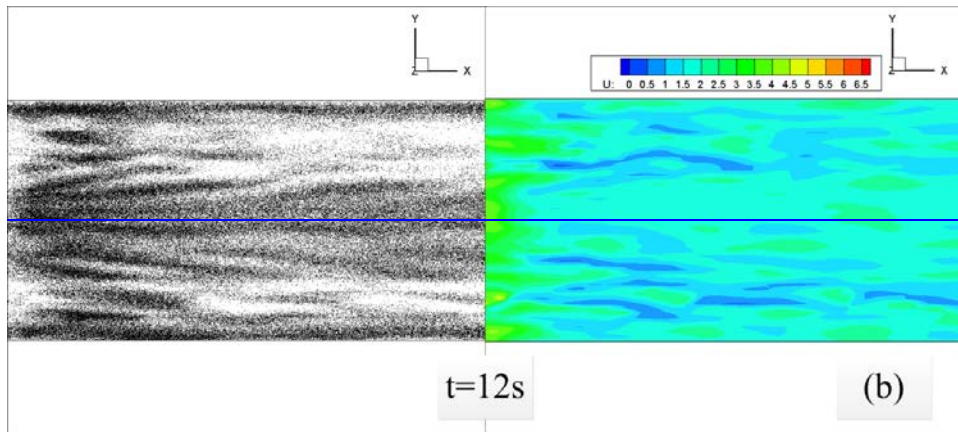
757

**Figure 10.** The TKE profile (a) and wind profile (b) at different time, in which the wind data between 13~15m along the downstream is used ( $u_s = 0.428 m / s$ ).

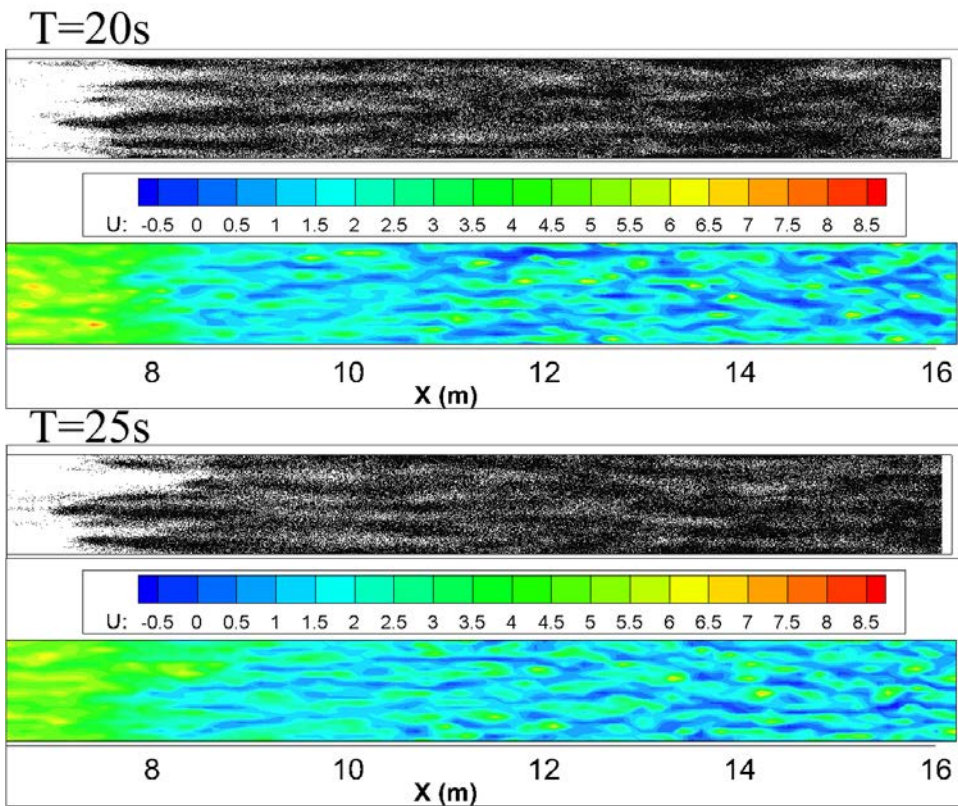
758



759

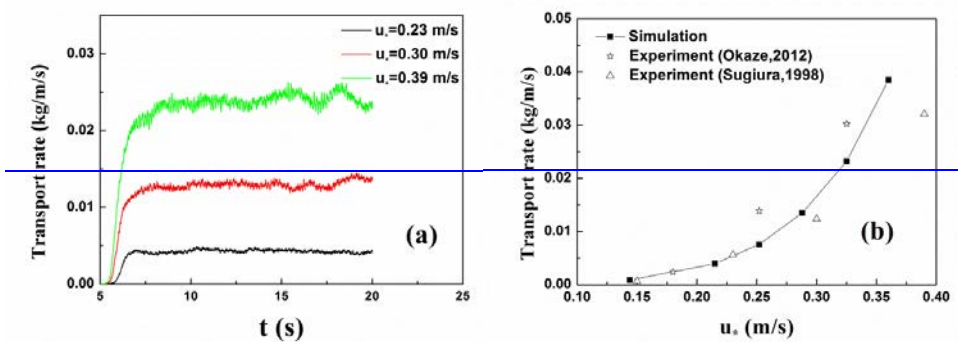


760



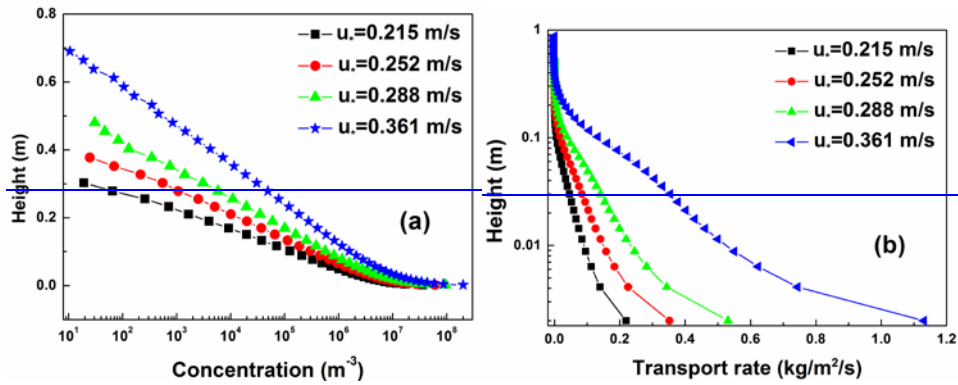
761

762 **Figure 611.** The top view of the particle concentration and the horizontal section of  
 763 wind velocity cloud map at corresponding moment ( $u_* = 0.357 \text{ m/s}$ , one dark spot  
 764 stands for a snow particle and the height of horizontal section is  $H = 0.001 \text{ m}$ ).



765

766 **Figure 7.** Variation of the snow transport rate (STR) per width with (a) time and (b)  
 767 friction wind velocity.



带格式的：两端对齐

Figure 8. (a) The average particle concentrations and (b) STR per unit area versus the height at different friction wind velocities.

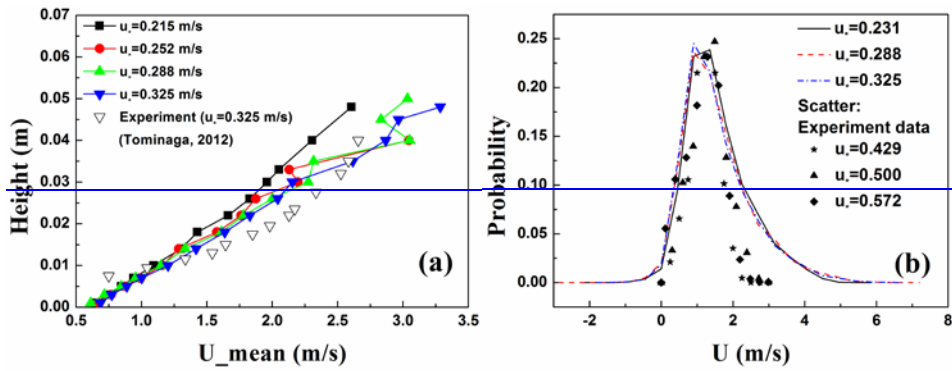
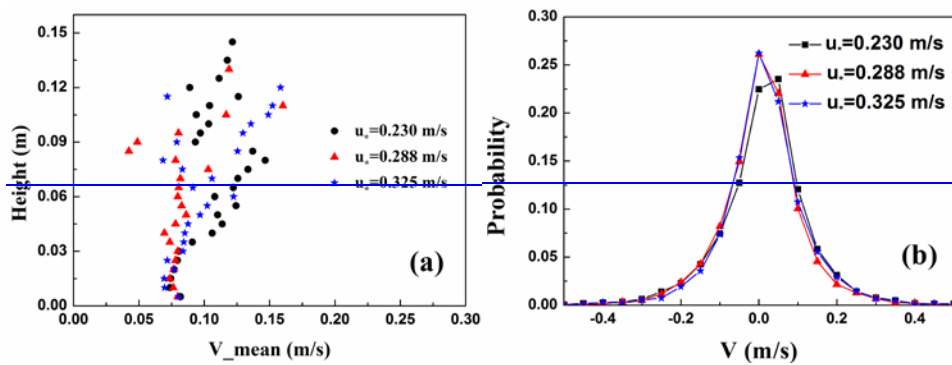
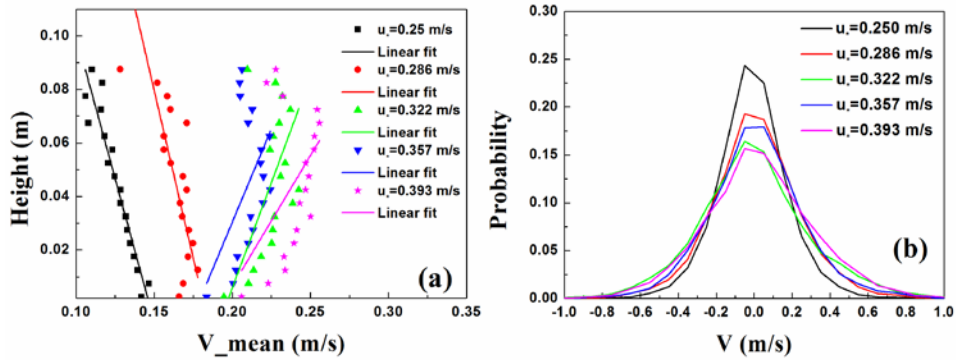


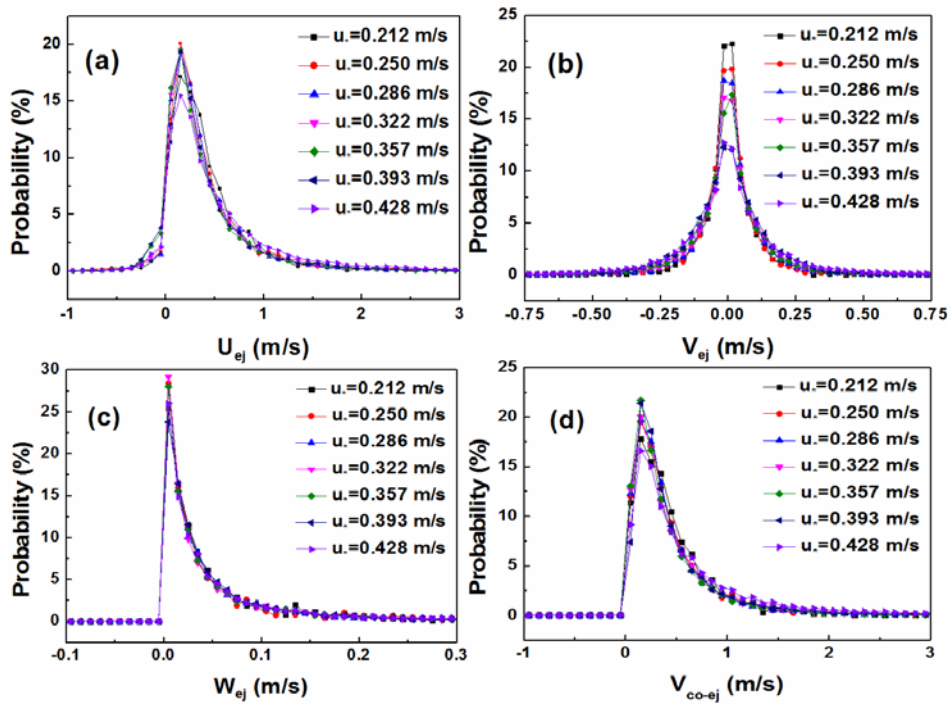
Figure 9. (a) Variation of the average velocity of snow particles along streamwise direction as a function of height and (b) the velocity probability distribution of snow particles.



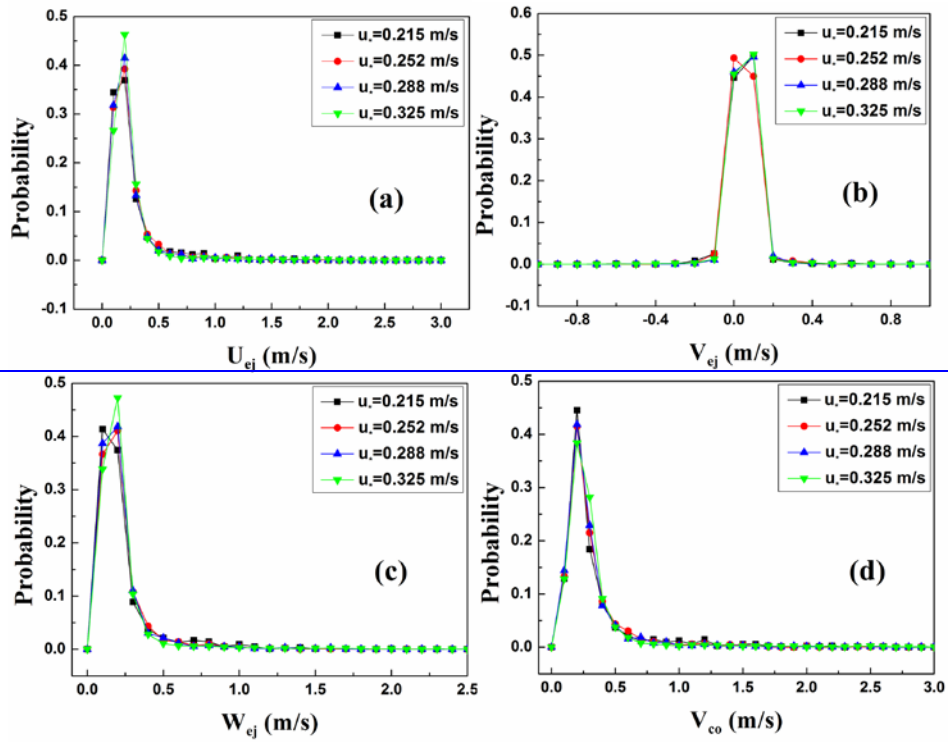


778  
779  
780  
781

**Figure 1012.** Distribution of (a) the absolute value of spanwise velocity along the elevation and (b) the corresponding probability distribution of snow particles in the air.

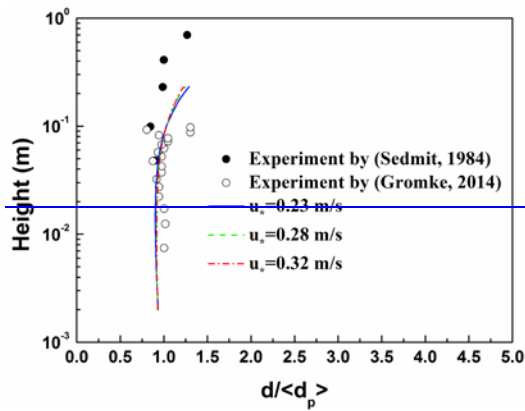


782



783  
784  
785

**Figure 11.** Distribution of the initial (a) streamwise, (b) spanwise, (c) vertical directions and (d) resultant take-off velocity of snow particles.



786  
787  
788

**Figure 12.** The mean equivalent diameter distribution of snow particles in the air vs height.